Applied Numerical Mathematics 2 (1986) 475–493
North-Holland

MULTIPLE GRID AND OSHER'S SCHEME FOR THE EFFICIENT SOLUTION OF THE STEADY EULER EQUATIONS

P.W. HEMKER and S.P. SPEKREIJSE
Centrum voor Wiskunde en Informatica, 1009 AB Amsterdam, The Netherlands

An iterative method is developed for the solution of the steady Euler equations for inviscid flow. The system of hyperbolic conservation laws is discretized by a finite-volume Osher-discretization. The iterative method is a multiple grid (FAS) iteration with symmetric Gauss–Seidel (SGS) as a relaxation method. Initial estimates are obtained by full multigrid (FMG). In the pointwise relaxation the equations are kept in block-coupled form and local linearization of the equations and the boundary conditions is considered. The efficient formulation of Osher's discretization of the 2-D non-isentropic steady Euler equations and its linearization is presented. The efficiency of FAS-SGS iteration is shown for a transonic model problem. It appears that, for the problem considered, the rate of convergence is almost independent of the gridsize and that for all meshsizes the discrete system is solved up to truncation error accuracy in only a few (2 or 3) iteration cycles.

1. Introduction

Recently the multiple grid method has become a well-established technique for the acceleration of relaxation-iterations to solve the sparse systems that arise from discretization of elliptic partial differential equations. The advantage of multigrid over other acceleration techniques is the fact that—under suitable, but quite general circumstances—the rate of convergence is independent of the size of the system to be solved. For other methods the rate slows down rapidly for finer discretizations when the systems get larger. This makes the multiple grid method superior to other methods—at least for very large elliptic systems.

With success the multiple grid technique has also been applied for other types of equations, such as parabolic partial differential equations and integral equations. Based on the pioneering work of Brandt [2] it is expected that by the multigrid method, for many equations, a sufficiently accurate approximate solution can be computed in an amount of work that is equivalent to a small number of evaluations of the (nonlinear) operator.

Also for the steady solution of hyperbolic equations, such as the time-dependent Euler equations, the multiple grid technique has been used for the acceleration of the solution process [6, 7, 16, 18]. In particular when no accurate representation of the time dependence is required, a suitable acceleration may be expected.

In this paper we treat some aspects of the solution of the steady Euler equations. We show that for a—nontrivial—standard model problem, multiple grid iteration yields again a process of which the rate of convergence is independent of the size of the system. The problem treated is the transonic flow of a gas in a channel with a circular bump. No special provisions are made with respect to the solution that is to be found. The shock is captured by the discretization. Experiments with the computation of flows around an airfoil show a similar behavior. However, for flows with a smaller Mach number the convergence rate of the multigrid iteration slightly decreases, cf. [5].

We treat the Euler equations for two dimensions. However, all techniques used can be extended in a straightforward way to the 3-D Euler equations.

In the following sections we give the details of the computational method. In Section 2 we treat the finite-volume technique for the conservative discretization of the system of conservation laws, and we describe the implementation of the Osher approximate Riemann-solver in some detail. This description shows that the implementation of Osher's scheme is not so complex as is generally believed, provided that the right dependent variables are used. Two variants of Osher's scheme are shown, one being somewhat less expensive than the version originally proposed.

In Section 3 the treatment of the different possible boundary conditions is given. Similarly to what is seen for elliptic boundary value problems, it seems essential for a straightforward multigrid approach to have a discretization of the boundary conditions which is completely consistent with the discretization of the interior of the domain. This might be a reason why Osher's scheme—based on Riemann-invariants, just as a proper boundary condition treatment does—combines so well with multiple grid.

In Section 4 we give a description of the linearization of the discretization. Here again a good choice of dependent variables gives a convenient description and leads to a rather simple implementation. The linearization might be used for the solution of the nonlinear discrete system. Then the linear multigrid technique may serve the efficient solution of the linear system that arise in a Newton-type process. This approach is taken by Mulder [10]. In the present paper we use linearization in the nonlinear pointwise relaxation method. In each point the 4×4 nonlinear systems are approximately solved by one or more iterations of a Newton-process.

In Section 5 the FAS- and FMG-multigrid techniques are described and in Section 6 numerical results are shown. In the last section some conclusions are summarized.

2. Finite volume Osher discretization for the 2-D steady Euler equations

The 2-D Euler equations can be written in conservative vector form as

$$\frac{\partial}{\partial t} q + \frac{\partial}{\partial x} f(q) + \frac{\partial}{\partial y} g(q) = 0 , \tag{2.1}$$

on an open $\Omega \subset \mathbb{R}^2$, where

$$q = \begin{pmatrix} \rho \\ \rho u \\ \rho v \\ E \end{pmatrix}, \qquad f = \begin{pmatrix} \rho u \\ \rho u^2 + p \\ \rho uv \\ u(E+p) \end{pmatrix}, \qquad g = \begin{pmatrix} \rho v \\ \rho vu \\ \rho v^2 + p \\ v(E+p) \end{pmatrix}. \tag{2.2}$$

Here ρ, u, v, p and E are respectively density, velocity components in the x- and y-directions, pressure and total energy per unit volume. Furthermore, E may be expressed as

$$E = \rho \cdot (e + \tfrac{1}{2}(u^2 + v^2)) , \tag{2.3}$$

where the specific internal energy e is related to the pressure and density by the perfect gas law

$$p = (\gamma - 1)\rho e\,, \tag{2.4}$$

with γ denoting the ratio of specific heats.

In (2.2) the state-vector q is given in the conservation variables: mass, momentum and energy per unit volume. In some cases the same state is more conveniently described by the variables (ρ, u, v, p) or by (c, u, v, z), where $c = \sqrt{\gamma p/\rho}$ is the local speed of sound and $z = \ln(p\rho^{-\gamma})$ is a measure for the specific entropy.

To discretize (2.1), the domain Ω is subdivided into disjunct quadrilateral cells $\Omega_{i,j}$ in a regular fashion such that

$$\Omega = \bigcup_{i,j} \Omega_{i,j}\,.$$

We restrict ourselves to subdivisions that are topologically equivalent with simple square meshes, such that $\Omega_{i,j}$ and $\Omega_{i,j\pm1}$ or $\Omega_{i\pm1,j}$ are neighboring cells. Further we denote the neighbors of $\Omega_{i,j}$ by $\Omega_{ij,k}$, $(k = \mathrm{N}, \mathrm{S}, \mathrm{E}, \mathrm{W})$, and a common wall between $\Omega_{i,j}$ and $\Omega_{ij,k}$ by $\Gamma_{ij,k} = \bar{\Omega}_{ij} \cap \bar{\Omega}_{ij,k}$. The restriction to this kind of regular geometry is not necessary for the discretization method but leads to simple data structures when the method is implemented.

By integration of (2.1) over $\Omega_{i,j}$ we obtain

$$\frac{\partial}{\partial t} \int\int_{\Omega_{i,j}} q \,\mathrm{d}x\,\mathrm{d}y + \int_{\partial\Omega_{i,j}} (f \cdot n_x + g \cdot n_y)\,\mathrm{d}s = 0 \tag{2.5a}$$

or

$$V_{ij} \frac{\partial}{\partial t} q_{ij} + \sum_k \int_{\Gamma_{ij,k}} (f \cdot n_x + g \cdot n_y)\,\mathrm{d}s = 0\,, \tag{2.5b}$$

where V_{ij} is the volume of cell $\Omega_{i,j}$ and q_{ij} is the mean value of q over $\Omega_{i,j}$. Further we introduce the notation

$$\int_{\Gamma_{ij,k}} (f \cdot n_x + g \cdot n_y)\,\mathrm{d}s = f_{ij,k} \cdot s_{ij,k}\,,$$

where $s_{ij,k}$ is the length of $\Gamma_{ij,k}$ and $f_{ij,k}$ is the mean flux outward $\Omega_{i,j}$ over the side $\Gamma_{ij,k}$. Now it is easy to see that, if $\Omega_{i,j}$ and $\Omega_{i',j'}$ are neighbors with a common side

$$\Gamma_{ij,k} = \Gamma_{i'j',k'}$$

then $s_{ij,k} = s_{i'j',k'}$ and $f_{ij,k} = -f_{i'j',k'}$. The space discretization of (2.1) is done according to the Godunov principle (cf. [4]): the state $q(t, x, y)$ is approximated by $q_{ij}(t)$ for all $\Omega_{i,j}$ and the mean fluxes $f_{ij,k}$ are approximated from the states in the adjacent cells. For this purpose, a computed flux $f_{ij,k}(q_{ij}, q_{ij,k})$ is introduced to replace $f_{ij,k}$. Thus we obtain the semi-discretization of (2.1):

$$V_{ij} \frac{\partial}{\partial t} q_{ij} = -\sum_k s_{ij,k} f_{ij,k}(q_{ij}, q_{ij,k})\,, \tag{2.6}$$

and for the steady equations we obtain the discrete system of equations

$$N_h(q_h) = 0\,, \tag{2.7}$$

which is short for

$$(N_h(q_h))_{ij} := \sum_k s_{ij,k} f_{ij,k}(q_{ij}, q_{ij,k}) = 0 \quad \text{for all } i, j\,.$$

If the cell Ω_{ij} is adjacent to the boundary of Ω, i.e. $\Gamma_{ij,k} \subset \partial\Omega$, then a state $q_{ij,k}$ is possibly not available. In that case $f_{ij,k}$ is computed from q_{ij} and the boundary conditions at $\Gamma_{ij,k}$.

The main difficulty in the discretization of (2.1) is the construction of a proper approximation $f_{ij,k}$ for a given q_{ij} and $q_{ij,k}$. A possible approach is to consider the state $q(t, x, y)$ at $t = t_0$ as piecewise constant over the cells Ω_{ij} and to compute (approximately) the fluxes over the walls as a quasi one-dimensional problem during a small time $(t_0, t_0 + \Delta t)$, by solving the Riemann-problem for gasdynamics [4, 17]. These fluxes are used as $f_{ij,k}(q_{ij}, q_{ij,k})$. Approximate Riemann-solvers have been proposed by Steger–Warming [19], van Leer [4, 20, 21], Roe [14, 15] and Osher [11, 12].

The possible irregularity of the mesh is easily dealt with by making use of the invariance of the Euler equations under rotation of the coordinate system for the independent variables x and y. Let the normal of a skew wall $\Gamma_{ij,k}$, directed from Ω_{ij} to $\Omega_{ij,k}$, be given by $(n_1, n_2) = (\cos\phi_{ij,k}, \sin\phi_{ij,k})$, then the simple local rotation

$$\begin{pmatrix} x' \\ y' \end{pmatrix} = \begin{pmatrix} n_1 & n_2 \\ -n_2 & n_1 \end{pmatrix} \cdot \begin{pmatrix} x \\ y \end{pmatrix}$$

reduces the computation of $f_{ij,k}$ to the approximate solution of the one-dimensional Riemann problem in the x-direction, i.e.

$$f_{ij,k} := f_{ij,k}(q_{ij}, q_{ij,k}) = T_{ij,k}^{-1} f(T_{ij,k} q_{ij}, T_{ij,k} q_{ij,k}) , \tag{2.8}$$

where

$$T_{ij,k} = \begin{pmatrix} 1 & 0 & 0 & 0 \\ 0 & n_1 & n_2 & 0 \\ 0 & -n_2 & n_1 & 0 \\ 0 & 0 & 0 & 1 \end{pmatrix} .$$

The *numerical flux function* f will be discussed later in this paper. We see that the geometrical data about the mesh, needed to set up equation (2.7) are only the quantities $s_{ij,k}$ and $\phi_{ij,k}$ for each cell wall. Handling the irregular mesh by this finite-volume approach, there is no need to introduce a transformation in the equations that are used. They remain simply in their form (2.1)–(2.2). Further it is immediately clear that—in this way—the discrete system is fully conservative, also for the nonuniform mesh.

An additional advantage of this finite-volume approach is that we can easily set up the residual $N_h(q_h)$ and its linearization $\mathrm{d}N_h(q_h)/\mathrm{d}q_h$ by assembling the contributions that are computed for each cell wall separately. This assembling procedure is completely analogous to the finite element technique, where the construction of the load vector and the stiffness matrix is done by assembling the element stiffness matrices.

In this paper Osher's approximate Riemann-solver is used for the numerical flux $f(q_0, q_1)$ in (2.8). In the remainder of this section we give a short description of this function. In fact, we distinguish two strongly related variants of it, viz. the O-(original) variant and the P-(physical) variant. The advantages of the Osher discretization procedure can be found e.g. in [11, 12]. Its main disadvantage seems its supposed complexity, when compared with other approximate Riemann solvers. The main objective of our exposition is to show that the scheme can be implemented in a simple and straightforward way. Further we need this description for further reference and to show (in Section 4) how its linearization is obtained in a convenient way.

According to Osher, in (2.8) the numerical flux function is defined by

$$f(q_0, q_1) = \tfrac{1}{2}\left\{ f(q_0) + f(q_1) - \int_{q_0}^{q_1} |f_q(w)|\, \mathrm{d}w \right\}, \tag{2.9}$$

where $|f_q(w)|$ is the absolute value of the matrix $f_q(w)$, as defined by

$$|f_q(w)| := R|\Lambda|R^{-1}.$$

Here $|\Lambda|$ is the diagonal matrix of the absolute values of the eigenvalues λ of $f_q(w)$. These eigenvalues form the diagonal matrix Λ in the eigenvalue–eigenvector decomposition

$$f_q(w) = R\Lambda R^{-1}.$$

In (2.9) the integration path is still to be defined, but we know that the matrix has a complete set of eigenvalues λ_k viz. $\lambda_1 = u - c$, $\lambda_2 = \lambda_3 = u$, $\lambda_4 = u + c$ (where $c = \sqrt{\gamma p/\rho}$ is the speed of sound) and a set of 3 corresponding eigenspaces R_1, $R_{2,3}$ and R_4.

The integral $\int_{q_0}^{q_1} |f_q(w)|\, \mathrm{d}w$ is computed along a path $q = q(s)$, $0 \leqslant s \leqslant 1$, $q(0) = q_0$, $q(1) = q_1$. This path is divided into subpaths Γ_k, $k = 1, 2, 3$, connecting the states $q_{(k-1)/3}$ and $q_{k/3}$. These subpaths Γ_k are constructed such that on Γ_k the direction of the path $\partial q(s)/\partial s$ is tangential to R_m, $m = m(k)$, an eigenvector. Feasible choices for $R_{m(k)}$ are given in Table 1.

Table 1
The choice $m(k)$ and (between brackets) the tangential eigenspace along Γ_k for Osher-type methods

	Variant O $m(k)$		Variant P $m(k)$	
$k = 1$	4	(R_4)	1	(R_1)
$k = 2$	2, 3	$(R_{2,3})$	2, 3	$(R_{2,3})$
$k = 3$	1	(R_1)	4	(R_4)

The states $q_{1/3}$ and $q_{2/3}$ are determined by means of the Riemann invariants $\psi_l^{m(k)}(q(s))$, $l \neq m$, $l = 1, 2, 3, 4$, which are invariant quantities along Γ_k. These $\psi_l^m(q)$, $m = 1, 2, 3, 4$, are

$$\begin{aligned} &\psi_3^4 = \psi_3^1 = v, && \psi_1^4 = \psi_4^1 = z, \\ &\psi_2^1 = u + 2c/(\gamma - 1), && \psi_2^4 = u - 2c/(\gamma - 1), \\ &\psi_1^2 = \psi_1^3 = u, && \psi_4^2 = \psi_4^3 = p, \end{aligned} \tag{2.10}$$

where $c = \sqrt{\gamma p/\rho}$, $z = \ln(p\rho^{-\gamma})$. Thus, $q_{1/3}$ and $q_{2/3}$ are determined from q_0 and q_1 by the equations

$$\psi_l^{m(k)}(q_{(k-1)/3}) = \psi_l^{m(k)}(q_{k/3}), \qquad k = 1, 2, 3, \quad l \neq m(k).$$

These are 8 equations for the 8 unknowns in $q_{1/3}$ and $q_{2/3}$.

Expressing the state q in the dependent variables u, v, c and z, we obtain directly $z_{1/3} = z_0$, $z_{2/3} = z_1$, $v_{1/3} = v_0$, $v_{2/3} = v_1$. Introducing $\alpha = \exp((z_1 - z_0)/(2\gamma))$, $p_{1/3} = p_{2/3}$ leads to

$$c_{2/3}/c_{1/3} = \exp((z_{2/3} - z_{1/3})/2\gamma) = \alpha, \tag{2.11}$$

and we arrive at the linear system

$$\begin{aligned} &u_{1/3} \pm 2c_{1/3}/(\gamma - 1) = u_0 \pm 2c_0/(\gamma - 1) =: \Psi_0, \\ &u_{2/3} \mp 2c_{2/3}/(\gamma - 1) = u_1 \mp 2c_1/(\gamma - 1) =: \Psi_1, \\ &c_{2/3} = \alpha \cdot c_{1/3}, \qquad u_{2/3} = u_{1/3}. \end{aligned} \tag{2.12}$$

Here, the upper sign stands for the P-variant and the lower sign for the O-variant of the Osher scheme. This convention will be used throughout the remainder of this paper.

A meaningful solution exists for the P-variant as long as no cavitation occurs ($\Psi_0 > \Psi_1$); for the O-variant the path $q_0 - q_{1/3} - q_{2/3} - q_1$ does not exist in the (unlikely) case of two states q_0 and q_1 for which $\Psi_1 > \Psi_0$. (Notice that the meaning of Ψ_0, Ψ_1 is different for the O- and P-variant!)

This system is easily solved as

$$\begin{aligned} c_{1/3} &= \pm\tfrac{1}{2}(\gamma-1)\cdot(\Psi_0-\Psi_1)/(1+\alpha)\,, \\ c_{2/3} &= \alpha\cdot c_{1/3}\,, \\ u_{1/2} &:= u_{1/3} = u_{2/3} = (\Psi_1+\alpha\Psi_0)/(1+\alpha)\,. \end{aligned} \tag{2.13}$$

The relevant eigenvalues at the points $q_{k/3}$, $k = 1, 2, 3$, are

$$\begin{aligned} \bar{\lambda}_0 &:= \lambda_{m(1)}(q_0) = u_0 \mp c_0\,, \\ \bar{\lambda}_{1/3} &:= \lambda_{m(1)}(q_{1/3}) = u_{1/3} \mp c_{1/3}\,, \\ \bar{\lambda}_{1/2} &:= \lambda_{m(2)}(q_{1/3}) = \lambda_{m(2)}(q_{2/3}) = u_{1/3} = u_{2/3}\,, \\ \bar{\lambda}_{2/3} &:= \lambda_{m(3)}(q_{2/3}) = u_{2/3} \pm c_{2/3}\,, \\ \bar{\lambda}_1 &:= \lambda_{m(3)}(q_1) = u_1 \pm c_1\,. \end{aligned} \tag{2.14}$$

Because $\lambda_{1,4}$ are genuinely nonlinear eigenvalues, $\lambda_{m(k)}$ is monotonous along Γ_k, $k = 1, 3$, and $\lambda_{m(k)}(q(s))$ changes sign at most once along these Γ_k. E.g. a sonic point q_{s1} with $\lambda_{m(1)}(q(s_1))$ exists on Γ_1 if $\bar{\lambda}_0 \cdot \bar{\lambda}_{1/3} \leq 0$. This sonic point is computed from the linear system

$$\begin{aligned} \nu_s &= \nu_0\,, \qquad u_s \mp c_s = 0\,, \\ z_s &= z_0\,, \qquad u_s \pm 2c_s/(\gamma-1) = \Psi_0\,. \end{aligned} \tag{2.15}$$

Similarly, a sonic point q_{s2} is found on Γ_3 if $\bar{\lambda}_{2/3} \cdot \bar{\lambda}_1 \leq 0$.

Along the path $q(s)$, $0 \leq s \leq 1$, $\lambda_{m(k)}(q(s))$ may change sign only at the points $q_{1/3}$ or $q_{2/3}$ and at sonic points q_{s1} or q_{s2} (if they occur).

Thus from (2.9) we obtain

$$\begin{aligned} f(q_0, q_1) = {} & f(q_0)(\operatorname{sign}(\bar{\lambda}_0)+1)/2 + f(q_{s1})(\operatorname{sign}(\bar{\lambda}_{1/3}) - \operatorname{sign}(\bar{\lambda}_0))/2 \\ & + f(q_{1/3})(\operatorname{sign}(\bar{\lambda}_{1/2}) - \operatorname{sign}(\bar{\lambda}_{1/3}))/2 \\ & + f(q_{2/3})(\operatorname{sign}(\bar{\lambda}_{2/3}) - \operatorname{sign}(\bar{\lambda}_{1/2}))/2 \\ & + f(q_{s2})(\operatorname{sign}(\bar{\lambda}_1) - \operatorname{sign}(\bar{\lambda}_{2/3}))/2 + f(q_1)(1 - \operatorname{sign}(\bar{\lambda}_1))/2\,. \end{aligned}$$

In most cases many eigenvalues $\bar{\lambda}$ will have equal signs and $f(q_0, q_1)$ is computed as the sum of only a few $f(q)$. Further we notice that $f(q_0, q_1)$ is a continuous function in all $\bar{\lambda}$'s and we see $\pm\bar{\lambda}_{1/3} \leq \pm\bar{\lambda}_{1/2} \leq \pm\bar{\lambda}_{2/3}$. Because of this continuity we may neglect the case of a zero eigenvalue $\bar{\lambda}$ and we compute the numerical flux as

$$
\begin{aligned}
f(q_0, q_1) = \ & \text{if } \bar{\lambda}_0 > 0 && \text{then } f(q_0) \\
& + \text{if } \bar{\lambda}_0 \cdot \bar{\lambda}_{1/3} < 0 && \text{then sign } (\bar{\lambda}_{1/3}) \cdot f(q_{s1}) \\
& + \text{if } \bar{\lambda}_{1/3} \cdot \bar{\lambda}_{1/2} < 0 && \text{then } \pm f(q_{1/3}) \\
& + \text{if } \bar{\lambda}_{1/2} \cdot \bar{\lambda}_{2/3} < 0 && \text{then } \pm f(q_{2/3}) \\
& + \text{if } \bar{\lambda}_{2/3} \cdot \bar{\lambda}_1 < 0 && \text{then sign } (\bar{\lambda}_1) \cdot f(q_{s2}) \\
& + \text{if } \bar{\lambda}_1 < 0 && \text{then } f(q_1) .
\end{aligned}
$$

This expression seems rather complex. However, if the ordered sequence $\bar{\lambda}_0$, $\bar{\lambda}_{1/3}$, $\bar{\lambda}_{1/2}$, $\bar{\lambda}_{2/3}$, $\bar{\lambda}_1$ can be split in two parts (possibly empty), the first of which contains only negative and the second only positive signs, then a $\hat{q}$ exists such that simply $f(q_0, q_1) = f(\hat{q})$. We identify this state $\hat{q}$ as the state of the gas *at* the cell wall. For physically realistic situations, in the O-variant this occurs only in the supersonic cases (all $\bar{\lambda}$'s positive or negative). Then the scheme corresponds to a pure upwinding scheme. For the P-variant, however, it occurs not only for these supersonic cases, but on a sonic line and for subsonic flow as well. If we exclude the unlikely cases that $u_{1/2} < 0$ and $u_0 - c_0 > 0$, or $u_{1/2} > 0$ and $u_1 + c_1 < 0$, for the P-variant numerical fluxes near a shock are the only ones for which $f(q_0, q_1)$ is found to be a sum of more (viz. 3) terms $f(q)$. This makes the P-variant attractive from the point of view of efficiency.

3. Boundary conditions

The flux of the conservative variables $f_{ij,k}$, at the boundary of the domain Ω is partially determined by q_{ij}, the state of the flow near the boundary and partially by the boundary conditions. To compute the value of these $f_{ij,k}$ we determine first the state $q_B = q_{ij,k}$ at the boundary $\partial\Omega$, depending on q_{ij} and on the boundary conditions. Then $f(q_{ij}, q_B)$, as described in Section 2, is used to compute the boundary flux.

In order to see what boundary conditions are required at the boundary for a properly posed problem, we first consider a time-dependent one-dimensional problem on a half-line

$$\partial q/\partial t + \partial f(q)/\partial t = 0 , \qquad t \geq 0 , \quad x \geq 0 . \tag{3.1}$$

In quasi-linear form we write (3.1) as

$$q_t + A(q) q_x = 0 , \tag{3.2}$$

where $A(q) = \mathrm{d}f/\mathrm{d}q$.

For the hyperbolic system (3.2), a complete set of real eigenvalues $\Lambda(q)$ and linearly independent eigenspaces $R(q)$ exists and we obtain

$$q_t + R(q)\Lambda(q)R^{-1}(q) q_x = 0 . \tag{3.3}$$

Assuming the existence of a $w(q)$ such that

$$\mathrm{d}w/\mathrm{d}q = R^{-1}(q) , \tag{3.4}$$

we find the uncoupled system

$$w_t + \Lambda(w) w_x = 0 . \tag{3.5}$$

Clearly, for any component w_i for which $\lambda_i \leq 0$, the value $w_i(t, 0)$, $t \geq 0$, is determined by $w_i(0, x)$, $x \geq 0$. For these components the characteristics leave the domain $x > 0$. However, for components for which $\lambda_i > 0$, characteristics enter the domain and boundary conditions are to be given; i.e. for each $\lambda_i > 0$ a boundary condition $B_i(w, t) = 0$ is required and the complete set of conditions should yield a non-singular $\mathrm{d}B_i/\mathrm{d}w_j$ for all variables w_j for which $\lambda_j > 0$. Returning to the original dependent variables q, this means that a set boundary conditions $B_i(q, t) = 0$ is required such that

$$(\mathrm{d}B_i/\mathrm{d}q) \cdot (\mathrm{d}q/\mathrm{d}w_j) = (\mathrm{d}B/\mathrm{d}q)R^+(q) \tag{3.6}$$

is non-singular.

$R(q) = \mathrm{d}q/\mathrm{d}w$ is the set of eigenvectors of $A(q)$ and $\{\mathrm{d}q/\mathrm{d}w_j \mid \lambda_j > 0\} = R^+(q)$ is the rectangular matrix of eigenvectors corresponding to the positive eigenvalues.

For the discretization of the 2-D problem (2.1) near the boundary, the boundary conditions are considered as locally one-dimensional. This is completely consistent with the discretization over internal cell walls as treated in Section 2.

To satisfy the boundary conditions in the discrete equations (2.7) we determine q_B, the state at the boundary, such that it satisfies the boundary conditions and the equality

$$f_{ij,k} = f(q_B) = f(q_B, q_{ij}) . \tag{3.7}$$

In view of (2.9) the second equality implies

$$\int_{q_B}^{q_{ij}} f_q(w)\, \mathrm{d}w = \int_{q_B}^{q_{ij}} |f_q(w)|\, \mathrm{d}w , \tag{3.8}$$

i.e. q_B should satisfy the boundary conditions and should be connected with q_{ij} by a path $q(s)$ such that

$$\lambda_{m(k)}(q(s)) \geq 0 . \tag{3.9}$$

Such a path can be constructed again as a sum of subpaths along eigenvectors, as described in Section 2 for q_{ij} and $q_{ij,k}$. Now only the eigenvectors corresponding to the positive eigenvalues can be used and the number of subpaths depends on the type of the boundary conditions (i.e. depends on the number of ingoing and outgoing characteristics). The endpoints of the Γ_k are computed by means of the Riemann invariants (as in Section 2) and the boundary data.

We consider 5 different cases:

(1) *Supersonic inflow*: All $\lambda > 0$. A full set of 4 boundary conditions is necessary; $B(q_B) = 0$ specifies q_B completely; q_B is independent of q_{ij}; $f(q_B, q_{ij}) = f(q_B)$.

(2) *Supersonic outflow*: All $\lambda < 0$. No boundary condition is to be specified; $q_B = q_{ij}$ satisfies the relation $f(q_B, q_{ij}) = (f(q_{ij})$.

(3) *Subsonic inflow*: $u - c = \lambda_1 < 0$, $u = \lambda_{2,3} > 0$, $u + c = \lambda_4 > 0$. The integration path follows $R_{2,3}(q)$ and $R_4(q)$. Here we can distinguish between two possibilities:

(a) variant (P): q_B is connected to an intermediate state q_I along $R_{2,3}(q)$ and q_I is connected to q_{ij} by $R_4(q)$; or

(b) an Osher path (variant O): q_B and q_I are connected by $R_4(q)$, and q_I and q_{ij} by $R_{2,3}$.

In both cases the determination of q_B and q_I involves 8 unknowns. Three boundary conditions are given and 5 relations of the type (2.10), viz. for ψ_3^4, ψ_2^4, ψ_1^4, ψ_4^3, ψ_1^3, are available. In order to satisfy (3.9) no sonic point may appear between q_B and q_{ij}.

(4) *Subsonic outflow*: $\lambda_1 < 0$, $\lambda_{2,3} < 0$, $\lambda_4 > 0$. The integration path runs along $R_4(q)$ and q_{ij} and q_B are connected by

$$\psi_l^4(q_{ij}) = \psi_l^4(q_B), \quad l = 1, 2, 3. \tag{3.10}$$

The single boundary condition $B(q_B) = 0$ and the 3 relations (3.10) determine q_B. Again, no sonic point may appear between q_B and q_{ij}.

(5) *Solid wall*: $\lambda_1 < 0$, $\lambda_{2,3} = 0$, $\lambda_4 > 0$. Here a q_B can be computed as in the case of subsonic outflow, where $u = 0$ serves as the boundary condition. However, this state at the boundary q_B is not uniquely determined. Any other state q_B' which shares the state variables p (pressure) and $u = 0$ with q_B satisfies the relation $f(q_B) = f(q_B') = f(q_B, q_{ij})$ as well. Now there are different boundary states, which—however—all infer the same boundary flux, i.e. they all satisfy our requirements.

Example (subsonic inflow). Assume that at a subsonic inflow left-end boundary u_B, v_B, z_B are given. In the cell near the boundary the state q_{ij} is given by $q_{ij} = (c_{ij}, u_{ij}, v_{ij}, z_{ij})^T$, which should satisfy $u_{ij} > 0$, $u_{ij} + c_{ij} > 0$. Then q_{ij} and q_B are related by paths along $R_{2,3}(q)$ and along $R_4(q)$. Let the intersection point of both paths be $q_I = (c_I, u_I, v_I, z_I)$. Two possibilities exist: either q_{ij} and q_I are connected by $R_{2,3}(q)$ and q_I and q_B by $R_4(q)$ (O-variant), or q_{ij} and q_I are connected by $R_4(q)$ and q_I and q_B by $R_{2,3}(q)$ (P-variant). Consider the latter possibility; we have the relations

$$u_I - 2c_I/(\gamma - 1) = u_{ij} - 2c_{ij}/(\gamma - 1),$$

$$u_I = u_B, \qquad p_I = p_B, \qquad v_I = v_{ij}, \qquad z_I = z_{ij}.$$

Thus, we find $u_I = u_B$, $v_I = v_{ij}$, $z_I = z_{ij}$, $c_I = c_{ij} - \frac{1}{2}(\gamma - 1)(u_{ij} - u_B)$; $p_B = p_I$ is calculated from c_I and z_I and finally c_B is obtained from p_B and z_B.

Example (subsonic outflow). Assume that at a subsonic outflow left-end boundary the pressure p is given. In the cell near the boundary the state q_{ij} is given by $q_{ij} = (c_{ij}, u_{ij}, v_{ij}, z_{ij})^T$, which should satisfy $u_{ij} < 0$, $u_{ij} - c_{ij} < 0$. Then q_{ij} and q_B are related by (3.10) yielding $v_{ij} = v_B$, $z_{ij} = z_B$, $u_{ij} - 2c_{ij}/(\gamma - 1) = u_B - 2c_B/(\gamma - 1)$. Together with the prescribed p_B this results in

$$q_B = (c_B, u_{ij} - 2(c_{ij} - c_B)/(\gamma - 1), v_{ij}, z_{ij}),$$

where

$$c_B = \sqrt{\gamma p_B/\rho_B} \quad \text{and} \quad \rho_B = (p_B\, e^{-z_{ij}})^{1/\gamma}.$$

In (3.6) we found for a properly posed problem the requirement of a nonsingular $(dB/dq)R^+(q)$ for the boundary conditions $B_i(q) = 0$. This provides us with a measure for the quality of the boundary conditions. We can quantify the well-posedness of a set of boundary conditions $B(q) = 0$ by the angle between the subspaces spanned by $R^+(q)$ and $(dB/dq)^T$. E.g. for subsonic outflow the angle between $\nabla B(q)$ and $R_4(q)$ determines the quality of the boundary condition.

4. Linearization

Both in the case of a complete linearization of (2.7) and in the case when only local linearization is applied in a nonlinear relaxation method, we need convenient expressions for $dN_h(q_h)/dq_h$. From (2.7) we obtain

$$\frac{\partial(N_h(q_h))_{ij}}{\partial q_{lm}} = \frac{\partial}{\partial q_{lm}} \cdot \sum_k f_{ij,k}(q_{ij}, q_{ij,k}) s_{ij,k} = \sum_k s_{ij,k} \frac{\partial}{\partial q_{lm}} f_{ij,k}(q_{ij}, q_{ij,k}) \tag{4.1}$$

$$= \sum_k s_{ij,k} \frac{\partial}{\partial q_{ij}} f_{ij,k}(q_{ij}, q_{ij,k}) \qquad \text{if } \Omega_{lm} = \Omega_{ij}\,, \tag{4.1a}$$

$$= s_{ij,k} \frac{\partial}{\partial q_{ij,k}} f_{ij,k}(q_{ij}, q_{ij,k}) \qquad \text{if } \Omega_{lm} = \Omega_{ij,k}\,, \tag{4.1b}$$

$$= 0 \qquad \text{otherwise}\,. \tag{4.1c}$$

Now, in view of (2.8), the computation of $\mathrm{d}N_h(q_h)/\mathrm{d}q_h$ reduces to evaluations of

$$f'_{(0)}(q_0, q_1) = \partial f(q_0, q_1)/\partial q_0 \quad \text{and} \quad f'_{(1)}(q_0, q_1) = \partial f(q_0, q_1)/\partial q_1\,.$$

A matrix $\mathrm{d}N_h(q_h)/\mathrm{d}q_h$ can be assembled per cell wall as explained for $N_h(q_h)$ in Section 2.

If in (4.1a) $q_{ij,k} = q_{\mathrm{B}}$ is a boundary state, then a relation $q_{ij,k} = q_{\mathrm{B}}(q_{ij})$ exists and the corresponding term in (4.1a) is to be read as

$$\begin{aligned} & s_{ij,k} \frac{\mathrm{d}}{\mathrm{d}q_{ij}} f_{ij,k}(q_{ij}, q_{ij,k}) \\ & = s_{ij,k} \frac{\mathrm{d}}{\mathrm{d}q_{ij}} f_{ij,k}(q_{ij}, q_{\mathrm{B}}(q_{ij})) \\ & = s_{ij,k} \frac{\mathrm{d}}{\mathrm{d}q_{ij}} \{T^{-1} f(Tq_{ij}, Tq_{\mathrm{B}}(q_{ij}))\} \\ & = s_{ij,k} T^{-1} f'_{(0)}(Tq_{ij}, Tq_{\mathrm{B}}) T + s_{ij,k} T^{-1} f'_{(1)}(Tq_{ij}, Tq_{\mathrm{B}}) T(\mathrm{d}q_{\mathrm{B}}/\mathrm{d}q_{ij})\,. \end{aligned} \tag{4.2}$$

Here T denotes $T_{ij,k}$ as in (2.8). The derivatives $\mathrm{d}q_{\mathrm{B}}/\mathrm{d}q_{ij}$ depend on the type of boundary condition and are in each case derived from the relations $q_{\mathrm{B}}(q_{ij})$ as described in Section 3.

We noticed already that the integration paths are easily expressed in the dependent variables u, v, c and z. The numerical flux and its partial derivatives are also conveniently expressed in these variables. The flux-vector $f = (\rho u, \rho u^2 + p, \rho uv, u(E+p))^{\mathrm{T}}$ is found as a function of $q = (c, u, v, z)^{\mathrm{T}}$ by noting that

$$\rho = (\mathrm{e}^{-z} c^2/\gamma)^{1/(\gamma-1)}\,, \qquad p = \rho c^2/\gamma\,,$$
$$E = \tfrac{1}{2}\rho(u^2 + v^2) + \rho c^2/\gamma(\gamma - 1)\,.$$

In these variables the Jacobian matrix of the flux

$$\frac{\mathrm{d}f}{\mathrm{d}q} = \frac{\partial(\rho u, \rho u^2 + p, \rho uv, u(E+p))}{\partial(c, u, v, z)}$$

reads as

$$f'(q) = \frac{\mathrm{d}f}{\mathrm{d}q} = \begin{pmatrix} h\rho u/c & \rho & 0 & -\tfrac{1}{2}h\rho u \\ h\rho(u^2 + c^2)/c & 2\rho u & 0 & -\tfrac{1}{2}h(\rho u^2 + p) \\ h\rho uv/c & \rho v & \rho u & -\tfrac{1}{2}h\rho uv \\ hu(E + p + \rho c^2)/c & \rho u^2 + E + p & \rho uv & -\tfrac{1}{2}hu(E+p) \end{pmatrix}, \tag{4.3}$$

where $h = 2/(\gamma - 1)$. In terms of this matrix, from (2.17) follows

$$\begin{aligned}\frac{\partial}{\partial q_0} f(q_0, q_1) = \quad & \text{if } \bar{\lambda}_0 > 0 && \text{then } f'(q_0)\\ & + \text{if } \bar{\lambda}_0 \cdot \bar{\lambda}_{1/3} < 0 && \text{then sign } (\bar{\lambda}_{1/3}) f'(q_{s1})(\partial q_{s1}/\partial q_0)\\ & + \text{if } \bar{\lambda}_{1/3} \cdot \bar{\lambda}_{1/2} < 0 && \text{then } \pm f'(q_{1/3})(\partial q_{1/3}/\partial q_0)\\ & + \text{if } \bar{\lambda}_{1/2} \cdot \bar{\lambda}_{2/3} < 0 && \text{then } \pm f'(q_{2/3})(\partial q_{2/3}/\partial q_0)\,.\end{aligned} \tag{4.4}$$

The derivatives $\partial q/\partial q_0$, $q = q_{s1}$, $q_{1/3}$, $q_{2/3}$, are derived from the differentiable relations (2.11)–(2.15), which yield

$$\begin{aligned}&\partial\alpha = -\frac{\alpha}{2\gamma}\,\partial z_0\,, \qquad \partial\Psi_0 = \partial u_0 \pm \frac{2}{\gamma-1}\,\partial c_0\,, \qquad \partial\Psi_1 = 0\,,\\ &\partial u_{1/2} = \frac{\alpha}{1+\alpha}\left[\partial\Psi_0 \mp \frac{1}{\gamma(\gamma-1)}\,c_{1/3}\,\partial z_0\right],\\ &\partial c_{1/3} = \mp\tfrac{1}{2}(\gamma-1)[\partial u_{1/2} - \partial\Psi_0]\,, \qquad \partial c_{2/3} = \pm\tfrac{1}{2}(\gamma-1)\,\partial u_{1/2}\,,\\ &\partial c_{s1} = \frac{\gamma-1}{\gamma+1}\left[\frac{2}{\gamma-1}\,\partial c_0 \pm \partial u_0\right], \qquad \partial u_{s1} = \pm\partial c_{s1}\,.\end{aligned} \tag{4.5}$$

Hence

$$\frac{\partial q_{s1}}{\partial q_0} = \begin{pmatrix} \frac{2}{(\gamma+1)} & \pm\frac{(\gamma-1)}{(\gamma+1)} & 0 & 0\\ \pm\frac{2}{(\gamma+1)} & \frac{(\gamma-1)}{(\gamma+1)} & 0 & 0\\ 0 & 0 & 1 & 0\\ 0 & 0 & 0 & 1 \end{pmatrix}, \tag{4.6a}$$

$$\frac{\partial q_{1/3}}{\partial q_0} = \begin{pmatrix} \frac{1}{\alpha+1} & \pm\frac{\gamma-1}{2(\alpha+1)} & 0 & \frac{1}{2\gamma}\cdot\frac{c_{2/3}}{\alpha+1}\\ \pm\frac{2}{\gamma-1}\cdot\frac{\alpha}{\alpha+1} & \frac{\alpha}{\alpha+1} & 0 & \mp\frac{1}{\gamma(\gamma-1)}\cdot\frac{c_{2/3}}{\alpha+1}\\ 0 & 0 & 1 & 0\\ 0 & 0 & 0 & 1 \end{pmatrix}, \tag{4.6b}$$

$$\frac{\partial q_{2/3}}{\partial q_0} = \frac{\alpha}{\alpha+1}\cdot\begin{pmatrix} 1 & \pm\frac{1}{2}(\gamma-1) & 0 & -\frac{c_{1/3}}{2\gamma}\\ \pm\frac{2}{\gamma-1} & 1 & 0 & \mp\frac{c_{1/3}}{\gamma(\gamma-1)}\\ 0 & 0 & 0 & 0\\ 0 & 0 & 0 & 0 \end{pmatrix} \tag{4.6c}$$

With the expressions (4.3), (4.4) and (4.6), the matrix $f'_{(0)}(q_0, q_1)$ is readily computed; $f'_{(1)}(q_0, q_1)$ is obtained similarly. For an efficient implementation of (4.4), a splitting of the matrices (4.6) in low rank matrices is possible. It appears that both Jacobian matrices $f'_{(0)}(q_0, q_1)$ and $f'_{(1)}(q_0, q_1)$ are continuous functions of q_0 and q_1 as long as $\bar{\lambda}_{1/2} = u_{1/3} = u_{2/3} \neq 0$.

5. Multigrid iteration

Recently several attempts have been made to apply multigrid techniques for the solution of stationary and non-stationary Euler equations. Relevant papers are by Ron-Ho Ni [16], Steger [18], Jespersen [7, 8], Jameson [6], Dick [3], and Mulder [10]. The improvements by multigrid acceleration range from moderate to significant. The authors use different discretization methods and different methods for the solution of the nonlinear system. The most significant improvement for the solution of the stationary equations seems to be obtained by Mulder and van Leer [22], who use van Leer's flux splitting for the discretization and a 'switched evolution-relaxation' (SER) scheme for the solution of the nonlinear system. The SER-scheme is a hybrid form of time-stepping (forward Euler) and Newton's method. In each step a linear system is to be solved and it is to this linear solution process that multigrid is applied. For this linear multigrid process (the correction scheme, CS, used to accelerate linear Gauss–Seidel relaxation) they find a significant acceleration.

For the advantages and the disadvantages of the use of multigrid to a linearized system or, as an alternative, to use nonlinear multigrid see Jespersen [8]. In the present paper we consider a nonlinear multigrid method for the solution of the nonlinear system (2.7) with an—at the moment arbitrary but small—right-hand side

$$N_h(q_h) = r_h \,. \tag{5.1}$$

We use iteration with the full approximation scheme (FAS), cf. [2]. For this we need a sequence of discretizations

$$N_{h_i}(q_{h_i})$$

with $h_1 > h_2 > \cdots > h_l = h$. For the meshwidth h_i we take $h_i = 2h_{i+1}$. For an irregular mesh we delete each second meshline to obtain the coarser grid.

One FAS cycle for the solution of (5.1) consists of the following steps:

Step 0. Start with an approximate solution q_h.

Step 1. Improve q_h by application of p nonlinear (pre-) relaxation iterations to $N_h(q_h) = r_h$.

Step 2. Compute the residual $N_h(q_h)$.

Step 3. Find an approximation, q_{2h}, of q_h on the next coarser grid. (Either use $q_{2h} = R_{2h,h}q_h$, where $R_{2h,h}$, is a restriction operator from the h-grid to the $2h$-grid, or use another previously obtained approximation q_{2h}.)

Step 4. Compute

$$r_{2h} = N_{2h}(q_{2h}) + \bar{R}_{2h,h}(r_h - N_h(q_h)) \,,$$

where $\bar{R}_{2h,h}$ is (another) restriction operator from the h-grid to the $2h$-grid.

Step 5. Approximate the solution of

$$N_{2h}(q_{2h}) = r_{2h} \tag{5.2}$$

by application of σ FAS cycles. The result is called $\tilde{q}_{2h}$.

Step 6. Correct the current solution by

$$q_h := q_h + P_{h,2h}(\tilde{q}_{2h} - q_{2h}) \,,$$

where $P_{h,2h}$ is a prolongation (interpolation) operator.

Step 7. Improve q_h by application of q nonlinear (post-) relaxation iterations to $N_h(q_h) = r_h$.

The Steps 2–6 in this process are called 'coarse grid correction'. These steps are skipped on ɔ coarsest grid h_1. For the solution of the nonlinear system (2.7), FAS iteration is simply plied with $r_h = 0$ on the finest grid. By the FAS iteration in (5.2) small right-hand sides equal zero appear on the coarser grids.

In order to complete the description of the FAS-cycle we need to be explicit about:

(1) the choice of the operators N_{2h}, $P_{h,2h}$, $\bar{R}_{2h,h}$ and eventually $R_{2h,h}$;

(2) the FAS strategy, i.e. the numbers p, q, σ ($\sigma = 1$ characterizes a V-cycle, $\sigma = 2$ a -cycle);

(3) the nonlinear relaxation method.

For the operators N_{2h}, $P_{h,2h}$ and $R_{2h,h}$ we make a choice that is consistent with the concept our finite-volume discretization. This discretization is essentially a weighted residual ɔthod, where the solution is approximated by a piecewise constant function (on cells Ω_{ij}) d where the residual is weighted by characteristic functions on all Ω_{ij}. From this point of ɔw, it is natural to use a piecewise constant interpolation for $P_{h,2h}$ and to use addition over bcells for $\bar{R}_{2h,h}$ as in [10]. Notice that $\bar{R}_{2h,h} = P^{\mathrm{T}}_{h,2h}$. With these choices it is clear that

$$N_{2h}(q_{2h}) = \bar{R}_{2h,h} N_h (P_{h,2h} q_{2h}) , \tag{5.3}$$

. the coarse-grid finite-volume discretization is a formal Galerkin approximation of the e-grid finite-volume discretization. Using (5.3) on all different levels we obtain a nested quence of discretizations, i.e. the following scheme (Fig. 1) of operators and spaces is mmutative.

The effect of the Galerkin approximation $N_{2h} = \bar{R}_{2h,h} N_h P_{h,2h}$ on the approximate solution obtained after a coarse grid correction is the following. If we take $q_{2h} = R_{2h,h} q_h$ in Step 3 of e algorithm, with $R_{2h,h}$ such that $R_{2h,h} P_{h,2h} = I_{2h}$ is the identity operator on X_{2h}, and if (5.2) solved exactly, then

$$\bar{R}_{2h,h}[r_h - N_h P_{h,2h} R_{2h,h} \tilde{q}_h] = \bar{R}_{2h,h}[N_h q_h - N_h P_{h,2h} R_{2h,h} q_h] ,$$

, for the restriction of the residual

$$\bar{R}_{2h,h}[r_h - N_h(\tilde{q}_h)] = \bar{R}_{2h,h}[(N_h q_h - N_h P_{h,2h} R_{2h,h} q_h) - (N_h \tilde{q}_h - N_h P_{h,2h} R_{2h,h} \tilde{q}_h)] . \tag{5.4}$$

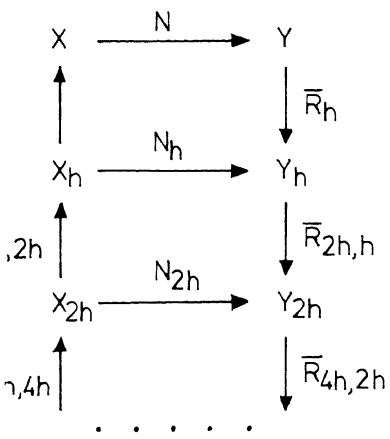

ɡ. 1. The nested sequence of discretizations.

In two particular cases the restriction of the residual vanishes for a Galerkin approximation. First, $q_h \in \text{Range}(P_{h,2h})$ implies $\tilde{q}_h \in \text{Range}(P_{h,2h})$. This means that for any such q_h the corrected solution $\tilde{q}_h$ has a residual for which the restriction vanishes:

$$\bar{R}_{2h,h}[r_h - N_h(\tilde{q}_h)] = 0 .$$

Secondly, for an affine operator N_h, (5.4) would imply

$$\bar{R}_{2h,h}N_h(I_h - P_{h,2h}R_{2h,h})(q_h - \tilde{q}_h) = \bar{R}_{2h,h}N_h(I_h - P_{h,2h}R_{2h,h})P_{h,2h} \cdots = 0 .$$

In the neighborhood of a solution, the difference $q_h - \tilde{q}_h$ will be small and N_h will approximately behave as an affine operator: the restriction of its residual will be very small, viz. $O(\| q_h - \tilde{q}_h \|^2)$. A small restriction of the residual means that possible large residues over neighboring cells cancel: the residual is rapidly varying. Local relaxation methods should be able to eliminate such residuals efficiently.

Experience with multigrid algorithms in another context makes it plausible that $p = q = \sigma = 1$ is a good choice for a strategy. This is the choice mainly used in our experiments. Other choices with small values for p, q and σ can be made. What is best depends much on the relaxation used, and research can be made seeking the most efficient combination. Up to now, it appears that different (p, q, σ)-strategies are not much different in efficiency. Usually a smaller convergence factor is compensated by a corresponding amount of additional work.

For the relaxation method we have used several alternatives, all being of the collective Gauss–Seidel type, where for each cell the 4 variables are recomputed simultaneously. For the solution of these nonlinear 4×4 systems, one or more steps of a Newton-iteration are used until the local residual is reduced below a specified amount. In almost all cases it appeared most efficient to take this tolerance so crude that no more than one iteration step per point is performed. Several relaxations were considered (cf. [5]): LEX: GS-relaxation with lexicographical ordering; SGS1: symmetric Gauss–Seidel from NW to SE and vice versa; SGS2: the same from NE to SW; RB: using a checkerboard ordering of the points. In almost all cases the same relaxation was used in both steps 1 and 7 of the algorithm. Another good choice was SGS3: to use SGS1 for the pre- and SGS2 for the post-relaxation. In [5] we compared some of these relaxations in combination with a uniform grid. In Section 6 we restrict ourselves to SGS3 relaxation and consider the effect of different strategies (p, q, σ).

For the nonlinear multigrid as described above, it is important to start with reasonably good initial estimates. Since we do not want to provide sophisticated a priori estimates, we use the full-multigrid (FMG) technique to compute this estimate.

In the FMG-method (or nested iteration) a crude initial estimate—in our case a uniform flow satisfying the inlet and outlet boundary conditions—is used. To obtain a first estimate on each finer level, first the solution on the next coarser grid is improved by a single FAS cycle and then this improved approximation is interpolated to the finer grid. These steps are repeated on the finer levels until the finest level has been reached.

The interpolation used to obtain the first guess on each level should be of high enough order to comply with the accuracy of the discretization. In our case, where the discretization is of first-order, the zero-order prolongation $P_{h,2h}$ as used in the Galerkin approximation is not accurate enough, and a first-order bilinear interpolation is used.

6. Numerical results

In this section, for a few numerical examples, we show that the rate of convergence of the

FAS-iteration is almost independent of the number of points in the mesh. Further, because the truncation error is $O(h)$ and the FAS convergence factors are well below 0.5, we see that with the FMG initial estimates a single (or a few) FAS iteration step(s) is (are) sufficient to obtain truncation error accuracy in the solution of the nonlinear system.

The examples used are based on a single physical problem: the computation of a transonic flow in a channel with a circular bump. This is a standard problem, used to compare many different methods [13].

The numerical experiments shown are restricted to the first-order discretization as described in Sections 2 and 3. We see that this discretization gives already a good approximation. Further improvement can be obtained by higher-order discretization. This, however, will not influence the rate of convergence of the FAS iteration, if the higher order is obtained by means of the defect correction [1], where only nonlinear systems of the type (5.1) are solved and the second order is obtained by the construction of the proper right-hand side r_h.

The physical problem is specified in Fig. 2. A non-uniform mesh in the channel is used as shown in Fig. 3.

At level l, $l = 1, 2, 3, 4, 5$ the vertices of the quadrangles Ω_{ij} in the (x, y)-space correspond to a regular square mesh over $5 \cdot 2^{(l-1)} \times 2 \cdot 2^{(l-1)}$ cells on $[-2, 3] \times [0, 2]$ in the (ξ, η)-space The (ξ, η) to (x, y) mapping is given by

$$\begin{cases} x = -0.42 - 0.15 \cdot \exp(-3.75\xi - 5.13), & -2.0 \leqslant \xi < -1.37, \\ x = 0.32\xi - 0.14, & -1.37 \leqslant \xi \leqslant 2.15, \\ x = 0.44 + 0.11 \cdot \exp(3.70\xi - 7.96), & 2.15 < \xi \leqslant 3.0. \end{cases}$$

$$\begin{cases} y = z, & |\xi| \geqslant 0.5, \\ y = z + 0.084(0.25 - x^2)(2 - z), & |\xi| < 0.5, \end{cases}$$

where $z = 0.19(\exp(1.222\eta) - 1.0)$.

In this case, where the bump is built in the geometry, both solid boundaries are treated as described in Section 3. This is in contrast with the approximation as used in [5] for uniform meshes.

In Fig. 3 both the pressure distribution along the lower and upper surface of the channel and the supersonic region in the channel are shown. We see that the shock extends over a single cell. In Fig. 4 we show the pressure distribution along the lower wall for various refinements of the mesh. In the finer discretization the Zierep expansion appears after the shock.

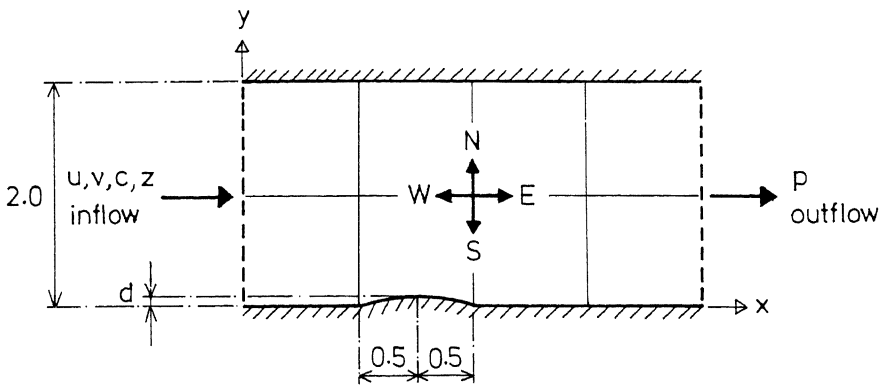

Fig. 2. The model problem: flow in a channel. The height of the circular bump is 0.042; $\gamma = 1.4$.

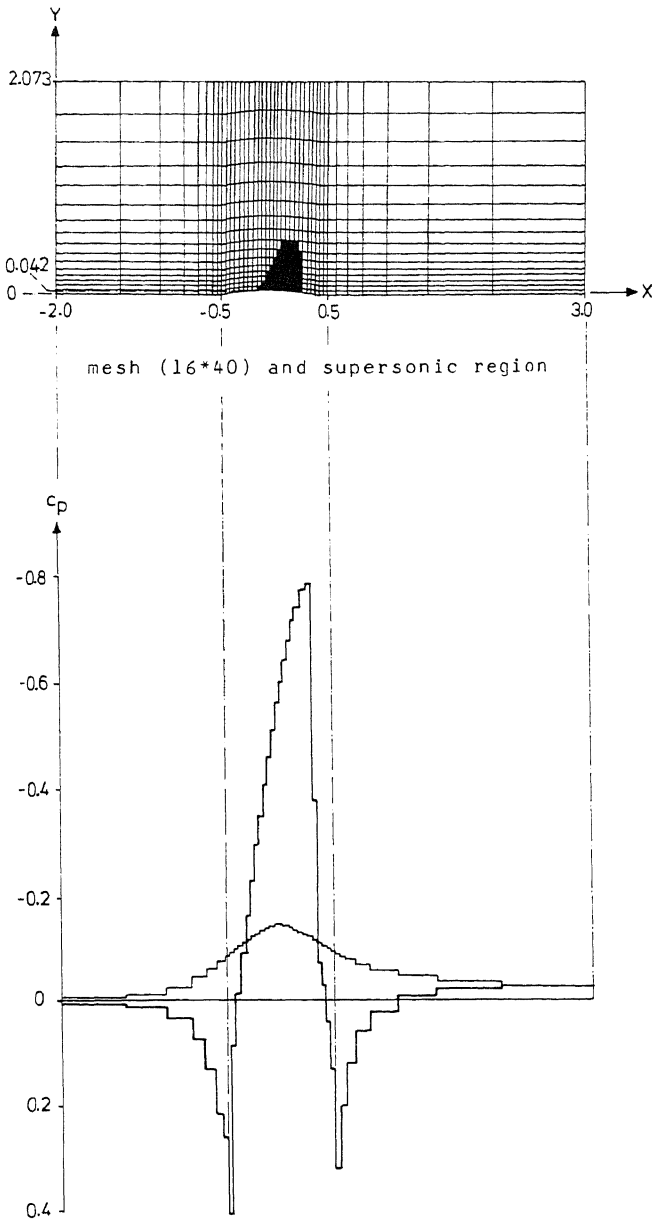

Fig. 3. The mesh at level 4 used for discretization of Ω. The supersonic region and the pressure distribution along the lower and upper surface are shown.

For the same problem, in Figs. 5–7 we show the convergence histories for several (p, q, σ)-strategies of the FAS iteration. The norm of the residual is shown after each iteration step. The norm used is the largest value of the L_1-norms of the four components in the flux. We see that the rate of convergence is almost independent of the number of levels. For the uniform mesh and the standard strategy [5] the convergence factor is about 0.25 per FAS-cycle and for the non-uniform mesh 0.38 per cycle. In all these experiments the P-variant of Osher's scheme was used. When the O-version was used, neither in the solution found, nor in the convergence behavior significant differences were observed.

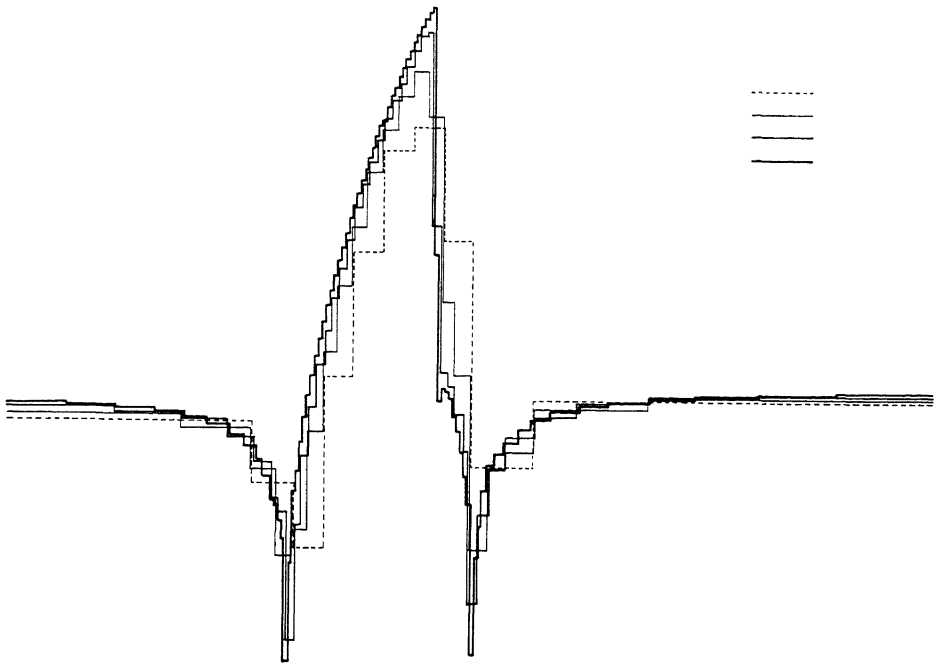

Fig. 4. The pressure distribution along the lower surface of the channel, computed for $l = 2, 3, 4, 5$.

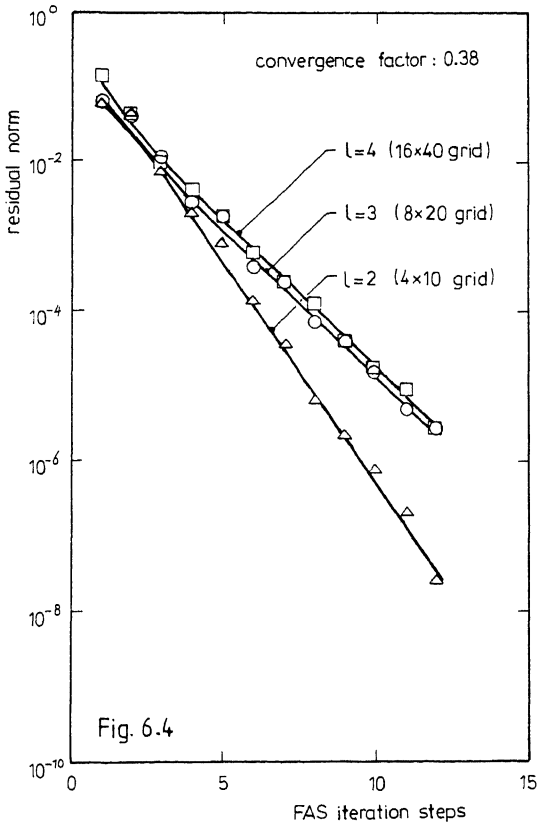

Fig. 5. The convergence history of the FAS iteration with strategy: $p = q = \sigma = 1$, and SGS3 iteration.

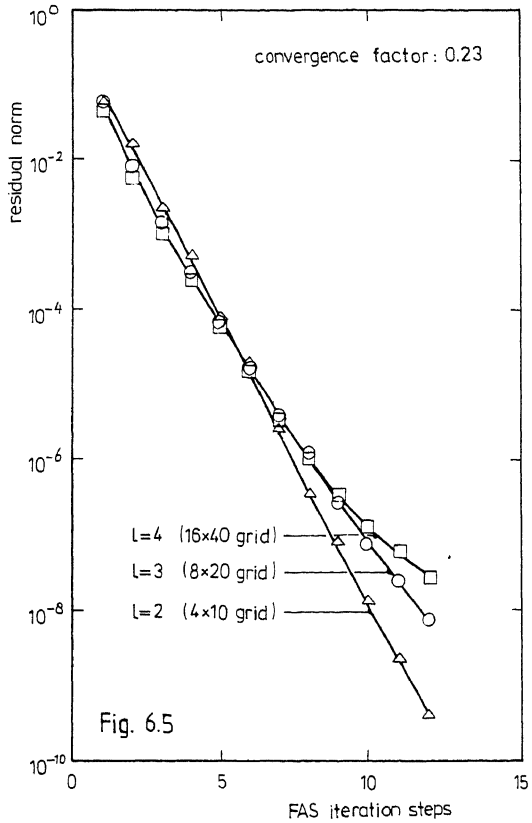

Fig. 6. The convergence history of the FAS iteration with strategy: $p = q = 1$, $\sigma = 2$, and SGS3 iteration.

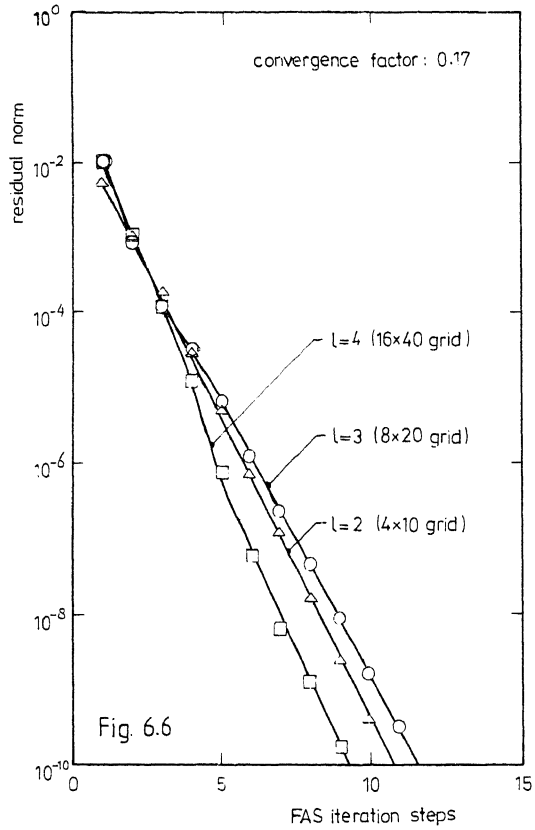

Fig. 7. The convergence history of the FAS iteration with strategy: $p = q = 2$, $\sigma = 1$, and SGS3 iteration.

7. Conclusion

In the previous sections we have seen—by a non-trivial example—that with a good sequence of discretizations real multigrid efficiency can be obtained for the transonic steady Euler equations, i.e. the rate of convergence for FAS iteration is independent of the number of cells in the mesh. A good sequence of discretizations is obtained by the consistent use of the finite-volume technique. It induces a completely conservative 2-D discretization and it prescribes both the prolongations and the restrictions. Moreover, it induces a sequence of Galerkin discretization on all grids.

Probably the most important ingredient in the finite-volume discretization is the choice of a good numerical flux function. For this Osher's approximate Riemann-solver, and a slight variant of it, could be used. The reason for the excellent performance might be the fact that a completely consistent treatment is given to the interior and the boundaries of the domain. Both at the domain boundaries and in the interior, the appropriate Riemann invariants are used to transfer information over cell boundaries. Further, the numerical flux has smooth derivatives, which avoids problems when Newton's method is used in the relaxation.

By the use of the FMG (full multigrid) technique, sufficiently accurate initial estimates could be obtained (for about the work of $\frac{1}{3}$ FAS-cycle) such that two or three FAS iterations (with $p = q = \sigma = 1$, SGS3-relaxation) are sufficient to obtain truncation error accuracy. This

means that these (non-isenthalpic and non-isentropic) steady Euler problems can be solved by an amount of work that is equivalent with about $3 \times \frac{4}{3} \times 2$ nonlinear symmetric Gauss–Seidel relaxations sweeps.

References

[1] K. Böhmer, P. Hemker and H. Stetter, The defect correction approach, *Computing Suppl. 5* (1984) 1–32.

[2] A. Brandt, Guide to multigrid development, in: W. Hackbusch and U. Trottenberg, eds., *Multigrid Methods*, Lecture Notes in Mathematics *960* (Springer, Berlin, 1982) 220–317.

[3] E. Dick, A multigrid method for the Cauchy–Riemann and steady state Euler equations based on flux difference splitting, in: W. Hackbusch, ed., *Efficient Solution in Elliptic Systems*, Proc. GAMM Seminar, Kiel, 1984 (Vieweg Verlag, 1984).

[4] A. Harten, P.D. Lax and B. van Leer, On upstream differencing and Godunov-type schemes for hyperbolic conservation laws, *SIAM Review 25* (1983) 35–61.

[5] P.W. Hemker and S.P. Spekreijse, Multigrid solution of the steady Euler equations, in: D. Braess, W. Hackbusch and U. Trottenberg, eds., *Advances in Multi-Grid Methods* (Vieweg Verlag, 1985).

[6] A. Jameson, Numerical solution of the Euler equations for compressible inviscid fluids, in: Proc. 6th International Conference on Computational Methods in Applied Science and Engineering, Versailles, France, 1983.

[7] D.C. Jespersen, Design and implementation of a multigrid code for the steady Euler equations, *Appl. Math. Comput. 13* (1983) 357–374.

[8] D.C. Jespersen, Recent developments in multigrid methods for the steady Euler equations. Lecture Notes, March 12–16, 1984, von Karman Inst., Rhode-St. Genese, Belgium.

[9] P.D. Lax, Hyperbolic systems of conservation laws and the mathematical theory of shock waves, Regional Conference Series in Applied Mathematics 11, SIAM Publication, 1973.

[10] W.A. Mulder, Multigrid relaxation for the Euler equations, *J. Comp. Phys. 60* (1985) 235–252.

[11] S. Osher and S. Chakravarthy, Upwind schemes and boundary conditions with applications to Euler equations in general geometries, *J. Comp. Phys. 50* (1983) 447–481.

[12] S. Osher and F. Solomon, Upwind difference schemes for hyperbolic systems of conservation laws, *Math. Comp. 38* (1982) 339–374.

[13] A. Rizzi and H. Viviand, eds., Numerical methods for the computation of inviscid transonic flows with shock waves, Proceedings GAMM Workshop, Stockholm, 1979 (Vieweg Verlag, 1981).

[14] P.L. Roe, Approximate Riemann solvers, parameter vectors and difference schemes, *J. Comp. Phys. 43* (1981) 357–372.

[15] P.L. Roe, The use of the Riemann problem in finite difference schemes, in: Reynolds and R.W. MacCormack, eds., *Proceedings Seventh International Conference on Numerical Methods in Fluid Dynamics*, Springer Lecture Notes in Physics *141* (Springer, Berlin/New York, 1981) 354–359.

[16] Ron-Ho Ni, A multiple grid scheme for solving the Euler equations, *AIAA Journal 20* (1982) 1565–1571.

[17] J. Smoller, Shock waves and reaction diffusion equations, Grundlehren der mathematische Wissenschaften *258* (Springer, Berlin/New York, 1983).

[18] J.L. Steger, A preliminary study of relaxation methods for the inviscid conservative gasdynamics equations using flux splitting, Nasa Contractor Report 3415 (1981).

[19] J.L. Steger and R.F. Warming, Flux vector splitting of the inviscid gasdynamics equations with applications to finite difference methods, *J. Comp. Phys. 40* (1981) 263–293.

[20] B. van Leer, Flux-vector splitting for the Euler equations, in: *Proceedings Eighth International Conference on Numerical Methods in Fluid Dynamics*, Lecture Notes in Physics *170* (Springer, Berlin/New York, 1982).

[21] B. van Leer, On the relation between the upwind-differencing schemes of Godunov, Engquist-Osher and Roe, *SIAM J. Num. Anal. 5* (1984) 1.

[22] B. van Leer and W.A. Mulder, Relaxation methods for hyperbolic conservation laws, in: F. Angrand, A. Dervieux, J.A. Desideri and R. Glowinski, eds., *Numerical Methods for the Euler Equations of Fluid Dynamics* (SIAM, Philadelphia, PA, 1985) 312–333.